Congreso de Métodos Numéricos en Ingeniería 2009
Barcelona, 29 junio al 2 de julio 2009

TWO-FLUID ELECTRO-OSMOTIC FLOWS OF VISCOELASTIC FLUIDS

Alexandre M. Afonso[1*], Manuel A. Alves[1] and Fernando T. Pinho[2]

1: CEFT
Departamento de Engenharia Química
Faculdade de Engenharia da Universidade do Porto
Rua Dr. Roberto Frias
4200-465 Porto, Portugal
e-mail: {aafonso, mmalves}@fe.up.pt, web: http://www.fe.up.pt/∼ceft/

2: CEFT
Departamento de Engenharia Mecânica
Faculdade de Engenharia da Universidade do Porto
Rua Dr. Roberto Frias, 4200-465 Porto, Portugal
e-mail: fpinho@fe.up.pt web: http://www.fe.up.pt/∼ceft/

Key words: Electro-osmotic flows; two-fluid pump; viscoelastic fluids.

Abstract. *Electro-osmotic flows (EOF) in microchannel systems have been studied extensively over the past decade, because they enable precise liquid manipulation in complex microchannel networks. Fluid pumps are indispensable elements in such microchannel networks,and promising candidates are electro-hydrodynamic pumps using ion-dragging effects via the so-called electro-osmosis, and travelling-wave-induced flow [1] due to the simplicity in producing small-sized pumps. This paper presents an analytical model that describes a two-fluid electro-osmotic flow of stratified viscoelastic fluids. This is the principle of operation of an EO two-fluid pump, recently presented [1, 2], in which an electrically nonconducting fluid is transported by the interfacial dragging viscous force of a conducting fluid that is driven by electro-osmosis. The electric potential in the conducting fluid and the analytical flow solution of the steady two-fluid electro-osmotic stratified flow in a planar microchannel are presented by assuming a planar interface between the two viscoelastic immiscible fluids. The effects of fluid rheology, dynamic viscosity ratio, holdup and interfacial zeta potential are analyzed to show the viability of this technique, where an enhancement of the flow rate is observed as the shear-thinning effects are increased.*

1 Introduction

Electro-osmotic flows (EOF) in microfluidic devices have been studied extensively over the past decade [1-5], because they enable precise liquid manipulation and are easily scalable to nanosized systems. The major applications of EO pumps are micro flow injection analysis, microfluidic liquid chromatography systems, microreactors, microenergy systems and microelectronic cooling systems. Fluid pumps are important elements in such microchannel networks, and promising candidates are electro-hydrodynamic pumps using ion-dragging effects via the so-called electro-osmosis, and traveling-wave-induced flow [1] due to the simplicity in producing small-sized pumps. A comprehensive review on electrokinetic pumps has been recently published by Wang et al [5].

Some of the above studies were focused on the transport of fluids with high electrical conductivity. For nonpolar fluids, such as oil, EOF pumping cannot be used, due to the low fluid conductivity [2]. To overcome this limitation, Brask et al [1] proposed an idea that allows the use of EOF as a driving mechanism, using an electric fluid with high conductivity to drag the low conductivity nonpolar fluid. Their study [1], analyzed the performance of the pump by equivalent circuit theory and computational fluid dynamic simulations.

The theoretical study of electro-osmotic flows of non-Newtonian fluids is recent and has been limited to simple inelastic fluid models, such as the power-law, due to the inherent analytical difficulties introduced by more complex constitutive equations. Examples are the recent works of Das and Chakraborty [6] and Chakraborty [7], who presented explicit relationships for velocity, temperature and concentration distributions in electro-osmotic microchannel flows of non-Newtonian bio-fluids described by the power-law model. Other purely viscous models were analytically investigated by Berli and Olivares [8], who considered the existence of a small wall layer depleted of additives and behaving as a Newtonian fluid (the skimming layer), under the combined action of pressure and electrical fields, thus restricting the non-Newtonian behaviour to the electrically neutral region outside the Electrical Double Layer (EDL).Very recently these studies were extended to viscoelastic fluids by Afonso et al [9], who presented analytical solutions for channel and pipe flows of viscoelastic fluids under the mixed influence of electrokinetic and pressure forces, using two constitutive models: the PTT model (Phan-Thien and Tanner [11]), with linear kernel for the stress coefficient function and zero second normal stress difference [12], and the FENE-P model, based on the kinetic theory for Finitely Extensible Non-linear Elastic dumbbells with a Peterlin approximation for the average spring force (cf. Bird et al [13]). Their analysis [9] was restricted to cases with small electric double-layers, where the distance between the walls of a microfluidic device is at least one order of magnitude larger than the EDL, and the fluid had a uniform distribution across the channel. When the viscoelastic flow is induced by a combination of both electric and pressure potentials, in addition to the single contributions from these two mechanisms there is an extra term in the velocity profile that simultaneously combines both forcings, which

is absent for the Newtonian fluids where the superposition principle applies. This extra term can contribute significantly to the total flow rate, depending on the value of the relative microchannel ratio and appears only when the rheological constitutive equation is non-linear. Afonso et al [14] extended this study to the flow of viscoelastic fluids under asymmetric zeta potential forcing.
The analytical solution of the steady two-fluid electro-osmotic stratified flow in a planar microchannel is presented here by assuming a planar interface between the two viscoelastic immiscible liquids. The PTT fluid [11] obeys the simplified model, with a linear kernel for the stress coefficient function [12] and has a zero second normal stress difference. The PTT model also includes the limiting case for Upper-Convected Maxwell (UCM) fluids.
The remaining of the paper starts with the flow problem definition, then is followed by the presentation of the set of governing equations and by the discussion of the assumptions made to obtain the analytical solution. Using this solution, the effects of the various relevant dimensionless parameters upon the flow field characteristics are discussed in detail.

2 Flow geometry and definitions

The flow under investigation is the steady, fully-developed flow of two incompressible and immiscible viscoelastic fluids as show schematically in Figure 1(a). This type of flow can be found in some EOF pumps [1], where the nonconducting fluid at the upper section of the system is dragged by an electrically conducting fluid at the bottom section, as illustrated in 1(b).

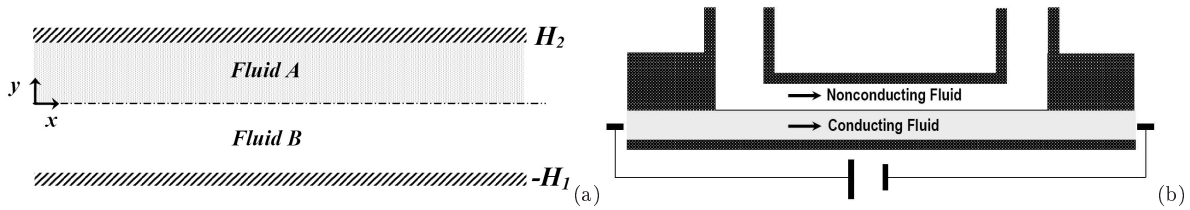

Figure 1: (a) Illustration of the coordinate system and (b) schematic of the two-fluid EOF pump.

The migration of ions naturally arises due to the interaction between the dielectric bottom wall and the conducting fluid. There is also dielectric interaction at the liquid-liquid interface leading to the formation of a second EDL in the conducting fluid next to the interface. Concerning the wall-fluid interface, the charged bottom wall of the channel attracts counter-ions to form a layer of charged fluid near the wall and repels the co-ions. A very thin layer of immobile counter-ions covers the bottom wall, known as the Stern layer, and is followed by a thicker more diffuse layer of mobile counter-ions, these two layers near the wall forming the EDL. The global charge of the conducting fluid remains neutral, but since the EDL is thin the core of the conducting fluid is essentially neutral. Applying a DC potential difference between the two electrodes at the inlet and outlet of the bottom channel section, generates an external electric field that exerts

a body force on the counter-ions of the EDL, which move along the bottom channel dragging the neutral conducting fluid core above. A similar situation arises at the fluid-fluid interface. There, the neutral conducting fluid (Fluid B) drags the nonconducting fluid (Fluid A) by the hydrodynamic viscous force at the interface (cf. Figure 1(a)). The pressure difference that can be independently applied between the inlets and outlets of both the upper and lower channels can act in the same or in the opposite directions of the electric field. Alternatively, the streamwise electric potential difference may not be imposed independently, but results from the accumulation of ions at the end of the channel due to the flow forced by an imposed pressure difference. This particular case is known as the streaming potential and implies a specific relationship between the imposed favorable pressure gradient and the ensuing adverse external electric field [15], a case which will not be analysed in this paper for conciseness.

To analyse this system, a two-dimensional Cartesian orthonormal coordinate system (x, y) is used with the origin located at the fluid-fluid interface, as shown in Figure 1(a). We assume a stratified viscoelastic flow and a planar interface, a condition satisfied when the contact angle between fluids A and B is close to 90^{o} [2]. The thickness of the conducting fluid is H_1 and that of the non-conducting fluid is H_2. The width w is assumed very large, such that $w \gg H_2 + H_1 = H$.

The holdup of the conducting fluid (Fluid B), R_B, is here defined as the ratio of the cross section area occupied by the conducting fluid to the cross section area of the channel, i.e.,

$$R_B = \frac{H_1}{H_2 + H_1} = \frac{H_1}{H} \tag{1}$$

Similarly, the hold up of nonconducting fluid (Fluid A) is defined as

$$R_A = 1 - R_B = \frac{H_2}{H_2 + H_1} = \frac{H_2}{H} \tag{2}$$

The electrical double layer forms near the bottom channel wall in contact with the conducting fluid (Fluid B) and has a zeta potential denoted by ζ_1. A second EDL can form in Fluid B in contact with fluid A and has an interfacial zeta potential (ζ_i) that depends on the properties of the two fluids and varies with the pH value, the concentration of ions in the conducting fluid and the presence of ionic surfactants [2]. This interface zeta potential influences the potential distribution in the EDL regions, hence the electroosmotic force distribution and therefore the flow.

3 Theoretical model of the two-fluid electroosmotic viscoelastic flow

The basic field equations describing this fully-developed flow of incompressible fluids are the continuity equation,

$$\nabla \cdot \mathbf{u} = 0 \tag{3}$$

and the modified Cauchy equation,

$$-\nabla p + \nabla \cdot \boldsymbol{\tau} + \rho_e \mathbf{E} = \mathbf{0} \tag{4}$$

where $\mathbf{u}$ is the velocity vector, p is the pressure and $\boldsymbol{\tau}$ is the polymeric extra-stress tensor. The $\rho_e\mathbf{E}$ term of equation (4) represents a body force per unit volume, where $\mathbf{E}$ is the applied external electric field and ρ_e is the net electric charge density in the fluid. This term is null for the non-polar fluid A. The main simplifying assumptions and considerations in the current analysis are: (i) the two fluids are viscoelastic (but the Newtonian fluid is also included as limiting case); (ii) fluid properties are assumed to be independent of local electric field, ion concentration and temperature (this is certainly true for dilute solutions [2], but we make this assumption for our fluids); (iii) the flow is steady and fully developed with no-slip boundary conditions at the channel walls; (iv) the two fluids are immiscible and there is stratification with a planar interface between fluids where an EDL can form; (v) a pressure gradient can simultaneously be imposed along the channel and (vi) standard electrokinetic theory conditions apply [10].

3.1 PTT model constitutive equations

The polymer extra-stress $\boldsymbol{\tau}$ is described by an appropriate constitutive equation, and in this work we consider the viscoelastic model of Phan-Thien and Tanner [11, 12] (PTT model) of equation (5) derived from network theory arguments

$$f(\tau_{kk})\boldsymbol{\tau} + \lambda\overset{\nabla}{\boldsymbol{\tau}} = 2\eta\mathbf{D} \tag{5}$$

Here $\mathbf{D} = \left(\bigtriangledown\mathbf{u}^T + \bigtriangledown\mathbf{u}\right)/2$ is the rate of deformation tensor, λ is the relaxation time of the fluid, η is the viscosity coefficient and $\overset{\nabla}{\boldsymbol{\tau}}$ represents the upper-convected derivative of $\boldsymbol{\tau}$, defined as

$$\overset{\nabla}{\boldsymbol{\tau}} = \frac{\mathrm{D}\boldsymbol{\tau}}{\mathrm{D}t} - \bigtriangledown\mathbf{u}^T.\boldsymbol{\tau} - \boldsymbol{\tau}.\bigtriangledown\mathbf{u}\,. \tag{6}$$

The stress coefficient function, $f(\tau_{kk})$, is given by the linear form [11]

$$f(\tau_{kk}) = 1 + \frac{\varepsilon\lambda}{\eta}\tau_{kk} \tag{7}$$

where τ_{kk} represents the trace of the extra-stress tensor and the maximum elongational viscosity is inversely proportional to a dimensionless parameter ε. For $\varepsilon = 0$ the UCM model is recovered which has an unbounded elongational viscosity. For fully-developed flow conditions, for which $\mathbf{u} = \{u(y), 0, 0\}$, the extra-stress field for the PTT model can be obtained from equations (5-7), leading to

$$f(\tau_{kk})\tau_{xx} = 2\lambda\dot{\gamma}\tau_{xy} \tag{8}$$

$$f(\tau_{kk})\tau_{xy} = \eta\dot{\gamma} \tag{9}$$

where $\tau_{kk} = \tau_{xx}$, since $\tau_{yy} = 0$ [16, 17], and $\dot{\gamma}$ is the transverse velocity gradient ($\dot{\gamma} \equiv du/dy$). Then, upon division of equation (8) by equation (9) the specific function $f(\tau_{xx})$

cancels out, and a relation between the normal and shear stresses is obtained,

$$\tau_{xx} = 2\frac{\lambda}{\eta}\tau_{xy}^2 \tag{10}$$

3.2 Electric double layers in the conducting fluid (Fluid B)

The potential field within the conducting fluid B, can be expressed by means of a Poisson–Boltzmann equation:

$$\nabla^2\psi = -\frac{\rho_e}{\epsilon} \tag{11}$$

where ψ denotes the electric potential and ϵ is the dielectric constant of the fluid. The net electric charge density, ρ_e, can be described as

$$\rho_e = -2n_o ez \sinh\left(\frac{ez}{k_B T}\psi\right) \tag{12}$$

where n_o is the ion density, e is the elementary electric charge, z is the valence of the ions, k_B is the Boltzmann constant, and T is the absolute temperature. In order to obtain the velocity field for fluid B, we first need to determine the net charge density distribution (ρ_e). The charge density field can be calculated by combining equation (11), that reduces to

$$\frac{d^2\psi}{dy^2} = -\frac{\rho_e}{\epsilon} \tag{13}$$

under fully developed flow conditions, with equation (12) to obtain the well-known Poisson–Boltzmann equation

$$\frac{d^2\psi}{dy^2} = \frac{2n_o ez}{\epsilon}\sinh\left(\frac{ez}{k_B T}\psi\right) \tag{14}$$

The electroosmotic flow is primarily caused by the action of an externally applied electric field on the charged species that exist near the bottom channel wall and in the vicinity of the interfacial surface. The distribution of the charged species in the domain is governed by the potentials at the wall and at the interface, and then by the externally applied electric field. When the Debye thicknesses are small and the charges at the wall and at the interface are not large, the distribution of the charged species is governed mainly by the ζ_1 potential at the wall and by ζ_i at the interface, and is affected very little by the external electric field (standard electrokinetic theory). Thus, the charge distribution across fluid B, can be determined independently of the externally applied electric field. Indeed, the effect of fluid motion on the charge redistribution can be neglected when the fluid velocity is small, i.e., when the inertial terms in the momentum equation are not dominant (they are null under fully developed conditions) or when the Debye thickness is small. Then, for small values of ψ, the Debye–Hückle linearization principle ($\sinh x \approx x$) can also be used, which means physically that the electric potential energy is small compared with

the thermal energy of ions, and the Poisson–Boltzmann equation can be transformed into the following form:

$$\frac{d^2\psi}{dy^2} = \kappa^2\psi \tag{15}$$

where $\kappa^2 = \frac{2n_o e^2 z^2}{\epsilon k_B T}$ is the Debye–Hückel parameter, related with the thickness of the Debye layer as $\xi = \frac{1}{\kappa}$ (normally referred to as the EDL thickness). This approximation is valid when the Debye thickness is small but finite, i.e., for $10 \lesssim H_1/\xi \lesssim 10^3$.
Equation (15) can be integrated subjected to the following boundary conditions: zeta potential at the bottom wall $\psi_{\|y=-H_1} = \zeta_1$ and zeta potential at the interface $\psi_{\|y=0} = \zeta_i$. The potential field becomes

$$\psi(y) = \zeta_1 \left(\Psi_1 e^{\kappa y} - \Psi_2 e^{-\kappa y}\right) \tag{16}$$

for $-H_1 \leq y \leq 0$. Denoting $R_\zeta = \zeta_i/\zeta_1$ as the ratio of zeta potentials, then $\Psi_1 = \frac{R_\zeta e^{\kappa H_1} - 1}{e^{\kappa H_1} - e^{-\kappa H_1}}$ and $\Psi_2 = \frac{R_\zeta e^{-\kappa H_1} - 1}{e^{\kappa H_1} - e^{-\kappa H_1}}$. When $R_\zeta = 1$ the symmetric potential profile is that obtained by Afonso et al [9] whereas for vanishing zeta potential at the interface, $R_\zeta = 0$, one obtains that defined by Afonso et al [14]. Finally the net charge density distribution, equation (12), together with the Debye–Hückle linearization principle leads to

$$\rho_e = -\epsilon\kappa^2\zeta_1 \left(\Psi_1 e^{\kappa y} - \Psi_2 e^{-\kappa y}\right) = -\epsilon\kappa^2\zeta_1\Omega_1^-(y) \tag{17}$$

where the operator $\Omega_i^\pm(y) = \Psi_1^i e^{(\kappa y)^i} \pm \Psi_2^i e^{(-\kappa y)^i}$ is a hyperbolic function of the transverse variable y, and depends on the ratio of zeta potentials, R_ζ, and on the thickness of the Debye layer.

3.3 Momentum equation of the two-fluid flow

3.3.1 Conducting fluid (Fluid B)

For the conducting fluid (Fluid B), the momentum equation (4), reduces to,

$$\frac{d\tau_{xy}^B}{dy} = p_{,x} - \rho_{\mathrm{e}}\mathrm{E_x} = p_{,x} + \epsilon\kappa^2\zeta_1 E_x \Omega_1^-(y) \tag{18}$$

where $E_x \equiv -\mathrm{d}\phi/\mathrm{d}x$ and $p_{,x} \equiv \mathrm{d}p/\mathrm{d}x$. The electric potential of the applied external field, ϕ, is characterized by a constant streamwise gradient. Equation (18) can be integrated to yield the following shear stress distribution

$$\tau_{xy}^B = p_{,x}y + \epsilon\kappa\zeta_1 E_x \Omega_1^+(y) + C_B \tag{19}$$

where C_B is an integration coefficient, that will be determined in section 3.3.3 from a boundary condition at the fluid-fluid interface. It is clear that in contrast to pure Poiseuille flow the shear stress distribution is no longer linear on the transverse coordinate. Using

the relationship between the normal stress and the shear stress, equation (10), an explicit expression for the normal stress component is obtained,

$$\tau_{xx}^{B} = 2\frac{\lambda}{\eta}\left(p_{,x}y + \epsilon\kappa\zeta_1 E_x \Omega_1^+(y) + C_B\right)^2 \tag{20}$$

For simplicity subscript B will be removed from the rheological parameters of Fluid B ($\eta_B = \eta$, $\varepsilon_B = \varepsilon$ and $\lambda_B = \lambda$). Combining (9), (19) and (20) we come to the expression for the velocity gradient

$$\dot{\gamma}^{B} = \left[1 + 2\varepsilon\lambda^2\left(\frac{\epsilon E_x\zeta_1}{\eta}\kappa\Omega_1^+(y) + \frac{C_B}{\eta} + \frac{p_{,x}}{\eta}y\right)^2\right]\left(\frac{\epsilon E_x\zeta_1}{\eta}\kappa\Omega_1^+(y) + \frac{C_B}{\eta} + \frac{p_{,x}}{\eta}y\right) \tag{21}$$

Equation (21) can be integrated subject to the no-slip boundary condition at the wall ($u^B_{\|y=-H_1} = 0$) leading to

$$\begin{aligned}
u^B = {} & \frac{C_B}{\eta}(y+H_1)\left(1 + 2\varepsilon\lambda^2\left(\frac{C_B}{\eta}\right)^2\right) + \left[\frac{\epsilon E_x\zeta_1}{\eta}\right]\left(1 + 6\varepsilon\lambda^2\left(\frac{C_B}{\eta}\right)^2\right)\Omega^-_{1,1}(y) + 2\frac{C_B}{\eta}\varepsilon\lambda^2\left[\frac{p_{,x}}{\eta}\right]^2(y^3 + H_1^3) \\
& + 2\varepsilon\lambda^2\left[\frac{\epsilon E_x\zeta_1}{\eta}\right]^2\kappa\left(\frac{C_B}{\eta}\left(6\Psi_1\Psi_2\kappa(y+H_1) + \frac{3}{2}\Omega^-_{2,1}(y)\right) + \left[\frac{\epsilon E_x\zeta_1}{\eta}\right]\kappa\left(\frac{1}{3}\Omega^-_{3,1}(y) + 3\Psi_1\Psi_2\Omega^-_{1,1}(y)\right)\right) \\
& + \frac{1}{2}\left[\frac{p_{,x}}{\eta}\right](y^2 - H_1^2)\left(1 + 6\varepsilon\lambda^2\left(\frac{C_B}{\eta}\right)^2 + \varepsilon\lambda^2\left[\frac{p_{,x}}{\eta}\right]^2(y^2 + H_1^2) + 24\frac{\varepsilon\lambda^2\left[\frac{\epsilon E_x\zeta_1}{\eta}\right]}{\kappa(y^2 - H_1^2)}\frac{C_B}{\eta}\left(\Omega^-_{1,2}(y) - \Omega^-_{1,1}(y)\right)\right) \\
& + 6\varepsilon\lambda^2\left[\frac{\epsilon E_x\zeta_1}{\eta}\right]^2\left[\frac{p_{,x}}{\eta}\right]\left(\Psi_1\Psi_2\kappa^2(y^2 - H_1^2) + \frac{1}{2}\Omega^-_{2,2}(y) - \frac{1}{4}\Omega^+_{2,1}(y) + \frac{\left[\frac{p_{,x}}{\eta}\right]}{\kappa^2\left[\frac{\epsilon E_x\zeta_1}{\eta}\right]}\left(\Omega^-_{1,3}(y) + 2\Omega^-_{1,1}(y) - 2\Omega^+_{1,2}(y)\right)\right)
\end{aligned} \tag{22}$$

where the operator $\Omega^{\pm}_{i,j}(y) \equiv (\kappa y)^{(j-1)}\,\Omega^{\pm}_i(y) - (-1)^{(j+1)}\,(\kappa H_1)^{(j-1)}\,\Omega^{\pm}_i(-H_1)$. This equation is valid for $-H_1 \le y < 0$.

It is often more convenient to work with the dimensionless form of equation (22). Introducing the normalizations $\bar{y} = y/H_1 = y/(R_B H)$ and $\bar{\kappa} = \kappa R_B H$, the dimensionless velocity profile in the conducting fluid can be written as

$$\begin{aligned}
\frac{u^B}{u_{sh}} = {} & \overline{C}_B(\overline{y}+1)\left(1 + 2\overline{C}_B^2\frac{\varepsilon De_\kappa^2}{\overline{\kappa}^2}\right) - \left(1 + 6\overline{C}_B^2\frac{\varepsilon De_\kappa^2}{\overline{\kappa}^2}\right)\Omega^-_{1,1}(y) + 2\overline{C}_B\frac{\varepsilon De_\kappa^2}{\overline{\kappa}^2}\Gamma^2\left(\overline{y}^3 + 1\right) \\
& + 2\overline{C}_B\frac{\varepsilon De_\kappa^2}{\overline{\kappa}}\left(6\Psi_1\Psi_2\overline{\kappa}(\overline{y}+1) + \frac{3}{2}\Omega^-_{2,1}(y)\right) - 2\varepsilon De_\kappa^2\left(\frac{1}{3}\Omega^-_{3,1}(y) + 3\Psi_1\Psi_2\Omega^-_{1,1}(y)\right) \\
& + \frac{1}{2}\Gamma\left(\overline{y}^2 - 1\right)\left(1 + 6\overline{C}_B^2\frac{\varepsilon De_\kappa^2}{\overline{\kappa}^2} + \frac{\varepsilon De_\kappa^2}{\overline{\kappa}^2}\Gamma^2\left(\overline{y}^2 + 1\right)\right) - 12\overline{C}_B\frac{\varepsilon De_\kappa^2}{\overline{\kappa}^3}\Gamma\left(\Omega^-_{1,2}(y) - \Omega^-_{1,1}(y)\right) \\
& + 6\frac{\varepsilon De_\kappa^2}{\overline{\kappa}^2}\Gamma\left(\Psi_1\Psi_2\overline{\kappa}^2\left(\overline{y}^2 - 1\right) + \frac{1}{2}\Omega^-_{2,2}(y) - \frac{1}{4}\Omega^+_{2,1}(y)\right) - 6\frac{\varepsilon De_\kappa^2}{\overline{\kappa}^4}\Gamma^2\left(\Omega^-_{1,3}(y) + 2\Omega^-_{1,1}(y) - 2\Omega^+_{1,2}(y)\right)
\end{aligned} \tag{23}$$

where $\overline{C}_B = \frac{C_B}{\eta}\frac{R_B H}{u_{sh}}$ and $De_\kappa = \frac{\lambda u_{sh}}{\xi} = \lambda\kappa u_{sh}$ is the Deborah number based on the relaxation time of the conducting fluid (Fluid B), on the EDL thickness and on the Helmholtz-Smoluchowski electro-osmotic velocity, defined as $u_{sh} = -\frac{\epsilon\zeta_1 E_x}{\eta}$. The dimensionless parameter $\Gamma = -\frac{(R_B H)^2}{\epsilon\zeta_1}\frac{p_{,x}}{E_x}$ represents the ratio of pressure to electro-osmotic

driving forces. Note that for simplicity the above terms were based on the zeta potential at the bottom wall ($\psi_{\|y=H_1} = \zeta_1$), but could be based on the interfacial zeta potential using the ratio of zeta potentials: $u_{sh} = u_{shi}/R_\zeta$, $\Gamma = R_\zeta \Gamma_i$ and $De_\kappa = De_{\kappa i}/R_\zeta$.
The flow rate can be determined from integration of the velocity profile of equation (22). Here, this integration was already carried out using the normalized velocity profile, equation (23), leading to the following expression for the normalized volumetric flow rate

$$\begin{aligned}
\overline{Q}^B = \frac{\overline{u}}{u_{sh}} = \frac{\int_{-H_1}^{0} u^B \mathrm{d}y}{u_{sh}} = {} & \frac{\overline{C}_B}{2} R_B H \left(1 + 2\frac{\varepsilon De_\kappa^2}{\overline{\kappa}^2}\overline{C}_B^2\right) - R_B H \left(1 + 6\frac{\varepsilon De_\kappa^2}{\overline{\kappa}^2}\overline{C}_B^2\right)\left(\frac{\Omega_{1,1}^+(0)}{\overline{\kappa}} - \Omega_1^-(-1)\right) \\
& + \frac{1}{2} R_B H \Gamma \left(-\frac{4}{5}\frac{\varepsilon De^2}{\overline{\kappa}^2}\Gamma^2 + \frac{2}{3}\left(1 + 6\overline{C}_B^2\frac{\varepsilon De^2}{\overline{\kappa}^2}\right)\right) \\
& + \frac{1}{2}\overline{C}_B R_B H \frac{\varepsilon De^2}{\overline{\kappa}^2}\left(3\Gamma^2 + 2\overline{\kappa}\left(6\Psi_1\Psi_2\overline{\kappa} + 3\left(\frac{\Omega_{2,1}^+(0)}{2\overline{\kappa}} - \Omega_2^-(-1)\right)\right)\right) \\
& - 2R_B H \varepsilon De_\kappa^2 \left(\frac{\Omega_{3,1}^+(0)}{9\overline{\kappa}} - \frac{1}{3}\Omega_3^-(-H_1) + 3\Psi_1\Psi_2\left(\frac{\Omega_{1,1}^+(0)}{\overline{\kappa}} - \Omega_1^-(-1)\right)\right) \\
& - 12R_B H \overline{C}_B \frac{\varepsilon De_\kappa^2}{\overline{\kappa}^3}\Gamma\left(\frac{1}{\overline{\kappa}}\left(\Omega_{1,2}^-(0) - \Omega_{1,1}^-(0) - \Omega_{1,1}^+(0)\right) + (\overline{\kappa}+1)\,\Omega_1^-(-1)\right) \\
& + 6R_B H \frac{\varepsilon De_\kappa^2}{\overline{\kappa}^2}\Gamma\left(\frac{1}{4\overline{\kappa}}\left(\Omega_{2,2}^+(0) - \Omega_{2,1}^-(0)\right) + \overline{\kappa}\Omega_2^-(-1) + \frac{1}{4}\Omega_2^+(-1) + \frac{2}{3}\Psi_1\Psi_2\overline{\kappa}^2\right) \\
& - 6R_B H \frac{\varepsilon De_\kappa^2}{\overline{\kappa}^4}\Gamma^2\left(\frac{1}{\overline{\kappa}}\left(\Omega_{2,3}^+(0) - 2\Omega_{1,2}^-(0) - 2\left(\Omega_{1,2}^+(0) - \Omega_{1,1}^+(0)\right)\right) + \left(\overline{\kappa}^2\Omega_1^-(-1) - 2\,(\overline{\kappa}+1)\,\Omega_1^+(-1)\right)\right)
\end{aligned} \tag{24}$$

3.3.2 Nonconducting fluid (Fluid A)

The derivation of the analytical solution follows the same steps as for the conducting fluid, with the necessary adaptations. For the nonconducting fluid (Fluid A), the momentum conservation equation (4), reduces to

$$\frac{d\tau_{xy}^A}{dy} = p_{,x} \tag{25}$$

since, as explained, the external electrical field forcing vanishes for this fluid. Equation (25) can be integrated to yield the following shear stress distribution

$$\tau_{xy}^A = p_{,x} y + C_A \tag{26}$$

where C_A is a boundary coefficient for the shear stress on Fluid A at the fluid-fluid interface, to be quantified in section 3.3.3. Using the relationship between the normal and shear stresses - equation (10), the following explicit expression for the normal stress component is obtained,

$$\tau_{xx}^A = 2\frac{\lambda_A}{\eta_A}\left(p_{,x} y + C_A\right)^2 \tag{27}$$

Combining equations (9), (26) and (27) the velocity gradient is given by

$$\dot{\gamma}^A = \left[1 + 2\varepsilon_A \lambda_A^2 \left(\frac{p_{,x}}{\eta_A} y + \frac{C_A}{\eta_A}\right)^2\right]\left(\frac{p_{,x}}{\eta_A} y + \frac{C_A}{\eta_A}\right) \tag{28}$$

Equation (28) is integrated subject to the no-slip boundary condition at the upper wall ($u^A_{\|y=H_2}=0$) and leads to

$$u^A = \frac{C_A}{\eta_A}(y-H_2)\left(1+2\varepsilon_A\lambda_A^2\left(\frac{C_A}{\eta_A}\right)^2\right)+2\varepsilon_A\lambda_A^2\frac{C_A}{\eta_A}\left[\frac{p_{,x}}{\eta_A}\right]^2\left(y^3-H_2^3\right) + \frac{1}{2}\left[\frac{p_{,x}}{\eta_A}\right]\left(y^2-H_2^2\right)\left(1+6\varepsilon_A\lambda_A^2\left(\frac{C_A}{\eta_A}\right)^2+\varepsilon_A\lambda_A^2\left[\frac{p_{,x}}{\eta_A}\right]^2\left(y^2+H_2^2\right)\right) \tag{29}$$

valid for $0<y\leq H_2$. Introducing the normalizations $\bar{y}=y/H_2=y/R_AH$ and $\bar{\kappa}_A=\kappa R_AH$, the dimensionless velocity profile can be written as

$$\frac{u^A}{u_{sh}} = \overline{C}_A(\overline{y}-1)\left(1+2\overline{C}_A^2\frac{\varepsilon_A De_{\kappa A}^2}{\overline{\kappa}_A^2}\right)+2\overline{C}_A\frac{1}{\beta^2}\frac{\varepsilon_A De_{\kappa A}^2}{\overline{\kappa}_A^2}\Gamma_A^2\left(\overline{y}^3-1\right) + \frac{1}{2}\frac{1}{\beta}\Gamma_A\left(\overline{y}^2-1\right)\left(1+6\overline{C}_A^2\frac{\varepsilon_A De_{\kappa A}^2}{\overline{\kappa}_A^2}+\frac{1}{\beta^2}\frac{\varepsilon_A De_{\kappa A}^2}{\overline{\kappa}_A^2}\Gamma_A^2\left(\overline{y}^2+1\right)\right) \tag{30}$$

where $\overline{C}_A=\frac{C_A}{\eta_A}\frac{R_AH}{u_{sh}}$, $\beta=\eta_A/\eta_B$ is the dynamic viscosity ratioand $De_{\kappa A}=\frac{\lambda_A u_{sh}}{\xi}=\lambda_A u_{sh}\kappa$ is the Deborah number based on the ralaxation time of fluid A, on the EDL thickness and on the Helmholtz-Smoluchowski electro-osmotic velocity. The parameter $\Gamma_A=-\frac{(R_AH)^2}{\epsilon\zeta_1}\frac{p_{,x}}{E_x}$ represents the ratio of pressure to electro-osmotic driving forces. The expression for the normalized volumetric flow rate of fluid A is

$$\overline{Q}^A=\frac{\overline{u}^A}{u_{sh}}=\frac{\int_0^{H_2}u^A\mathrm{d}y}{u_{sh}}=\frac{\overline{C}_A}{2}R_AH\left(1+2\frac{\varepsilon_A De_{\kappa A}^2}{\overline{\kappa}_A^2}\overline{C}_A^2\right) + \frac{1}{2}R_AH\frac{\varepsilon_A De_{\kappa A}^2}{\beta^2\overline{\kappa}_A^2}\Gamma_A^2\left(\overline{C}_A+\frac{1}{5}\frac{1}{\beta}\Gamma_A\right)+\frac{1}{6\beta}\Gamma_AR_AH\left(1+6\overline{C}_A^2\frac{\varepsilon_A De_{\kappa A}^2}{\overline{\kappa}_A^2}\right) \tag{31}$$

3.3.3 Fluid A- Fluid B interface conditions

In deriving the shear stress profiles, equations (19) and (26), and all the subsequent quantities like velocity and flow rates, two integration coefficients appeared, $\overline{C}_A$ and $\overline{C}_B$, which have to be determined from the boundary conditions at the fluid-fluid interface: ${\tau_{xy}}^A_{\|y=0}={\tau_{xy}}^B_{\|y=0}$ and $u^A_{\|y=0}=u^B_{\|y=0}$.

Using the relationships between the shear stresses at the interface, equations (19) and (26), and those for the dimensionless velocity profiles, equations (23) and (30), we arrive at a set of two equations for variables $\overline{C}_A$ and $\overline{C}_B$,

$$\begin{cases}\overline{C}_A=\frac{R_A}{R_B}\frac{1}{\beta}\overline{C}_B-\frac{\overline{\kappa}_A}{\beta}\Omega_1^+(0)\\ \overline{C}_B=\sqrt[3]{-\frac{b_1}{2}+\sqrt{\frac{b_1^2}{4}+\frac{a^3}{27}}}+\sqrt[3]{-\frac{b_1}{2}-\sqrt{\frac{b_1^2}{4}+\frac{a^3}{27}}}-\frac{a_1}{3}\end{cases} \tag{32}$$

where $a = a_2 - a_1^2/3$, $b_1 = a_3 - a_1 a_2/3 + 2a_1^3/27$, the coefficients a_1, a_2 and a_3 are given by

$$
\begin{aligned}
a_1 &= \frac{\frac{3}{2}\frac{\Gamma_A}{\beta^2} - \frac{3}{2}R_\varepsilon^2\frac{\overline{\kappa}_A^2}{\overline{\kappa}^2}\Gamma - 2R_\varepsilon^2\frac{\overline{\kappa}_A^2}{\overline{\kappa}^2}\Omega_{1,1}^-(0) - 3\frac{\overline{\kappa}_A}{\beta^3}\Omega_1^+(0)}{a_4} \\
a_2 &= \frac{\frac{1}{2}\frac{\overline{\kappa}_A^2}{\varepsilon_A De_{\kappa A}^2}\left(\frac{\beta+1}{\beta}\right) + R_\varepsilon^2\frac{\overline{\kappa}_A^2}{\overline{\kappa}^2}\Gamma^2 + R_\varepsilon^2\frac{\overline{\kappa}_A^2}{\overline{\kappa}^2}\left(6AB\overline{\kappa} + \frac{3}{2}\Omega_{2,1}^-(0)\right)}{a_4} \\
&+ \frac{\frac{\Gamma_A^2}{\beta} - 3\frac{\overline{\kappa}_A}{\beta^2}\Gamma_A\Omega_1^+(0) + 3\frac{\overline{\kappa}_A^2}{\beta^3}\left(\Omega_1^+(0)\right)^2 - 6R_\varepsilon^2\frac{\overline{\kappa}_A^2}{\overline{\kappa}^3}\Gamma\left(\Omega_{1,2}^-(0) - \Omega_{1,1}^-(0)\right)}{a_4} \\
a_3 &= \frac{\frac{1}{4}\Gamma_A\left(1+\Gamma_A^2\right) - \frac{1}{4}R_\varepsilon^2\frac{\overline{\kappa}_A^2}{\overline{\kappa}^2}\Gamma\left(1+\Gamma^2\right) - \frac{1}{2}\frac{\overline{\kappa}_A^2}{\varepsilon_A De_{\kappa A}^2}\left(\Omega_{1,1}^-(0) - \frac{\overline{\kappa_A}}{\beta}\Omega_1^+(0)\right)}{a_4} \\
&+ \frac{3R_\varepsilon^2\frac{\overline{\kappa}_A^2}{\overline{\kappa}^2}\Gamma\left(-AB\overline{\kappa}^2 + \frac{1}{2}\Omega_{2,2}^-(0) - \frac{1}{4}\Omega_{2,1}^+(0) - \frac{\Gamma}{\overline{\kappa}^2}\left(\Omega_{1,3}^-(0) + 2\Omega_{1,1}^-(0) - 2\Omega_{1,2}^+(0)\right)\right)}{a_4} \\
&- \frac{\frac{\overline{\kappa}_A}{\beta}\Omega_1^+(0)\left(\Gamma_A^2 - \frac{3}{2}\frac{\overline{\kappa}_A}{\beta}\Gamma_A\Omega_1^+(0) + \frac{\overline{\kappa}_A^2}{\beta^2}\left(\Omega_1^+(0)\right)^2\right) + R_\varepsilon^2\overline{\kappa}_A^2\left(\frac{1}{3}\Omega_{3,1}^-(0) + 3AB\Omega_{1,1}^-(0)\right)}{a_4}
\end{aligned}
\tag{33}
$$

$a_4 = \frac{1}{\beta^3} + R_\varepsilon^2\frac{\overline{\kappa}_A^2}{\overline{\kappa}^2}$ and $R_\varepsilon = \sqrt{\frac{\varepsilon}{\varepsilon_A}}\frac{\lambda^2}{\lambda_A^2}$ is a dimensionless number that relates the rheological properties of the two fluids.

4 Results and discussion

In the previous section, general equations were derived for steady fully developed two-fluid electro-osmotic stratified flow of PTT viscoelastic fluids under the mixed influence of electrokinetic and pressure gradient forces. The different influences of the driving forces (Γ), fluid rheology (R_ε), dynamic viscosity ratio (β), fluids holdup (R_A and R_B) and of the ratio of zeta potentials (R_ζ) on the velocity profile have been identified in equations (29), (22) and (32) and in this section we discuss in detail some limiting cases in order to understand the system fluid dynamics.

The following set of two-fluid systems is included in the general solution: (a) Newtonian-Newtonian fluid system; (b) viscoelastic-Newtonian fluid system; (c) Newtonian-viscoelastic fluid system; and (d) viscoelastic - viscoelastic fluid system. Cases (c) and (d) are not discussed in this work, due to space limitations, althougth the derived equations also include these cases. Case (a) was studied in detail elsewhere [2], but this situation is revisited here as a starting point and for comparison with case (b), i.e., in the following we analyse in detail the pumping of a Newtonian fluid by another Newtonian fluid, and, alternatively, by a viscoelastic fluid.

4.1 Newtonian-Newtonian EOF pump configuration

For the Newtonian-Newtonian flow configuration, both the conducting and nonconducting fluids are Newtonian, with zero relaxation times. The Deborah numbers vanish ($De_\kappa = De_{\kappa A} = 0$), and the velocity profile system equations and the dimensionless boundary condition coefficients, provided by equation (32), simplify to

$$\begin{cases} \frac{u^A}{u_{sh}} = \overline{C}_A\left(\overline{y}-1\right) + \frac{1}{2}\frac{1}{\beta}\Gamma_A\left(\overline{y}^2-1\right) & \text{for} \quad 0 \le \overline{y} \le 1 \\ \frac{u^B}{u_{sh}} = \overline{C}_B\left(\overline{y}+1\right) - \Omega^-_{1,1}(y) + \frac{1}{2}\Gamma\left(\overline{y}^2-1\right) & \text{for} \quad -1 \le \overline{y} \le 0 \\ \overline{C}_A = \frac{R_A}{R_B}\left(\frac{\Omega^-_{1,1}(0)+\frac{1}{2}\Gamma_A-\frac{1}{2}\Gamma+\frac{\overline{\kappa}}{\beta}\Omega^+_1(0)}{\left(1+\beta\frac{R_B}{R_A}\right)}\right) - \frac{\overline{\kappa}_A}{\beta}\Omega^+_1(0) \\ \overline{C}_B = \frac{\Omega^-_{1,1}(0)+\frac{1}{2}\Gamma_A-\frac{1}{2}\Gamma+\frac{\overline{\kappa}}{\beta}\Omega^+_1(0)}{\left(\frac{1}{\beta}+\frac{R_B}{R_A}\right)} \end{cases} \tag{34}$$

For small relative microchannel ratio, $\bar{\kappa} \to 1$, the double layer thickness is of the same order of magnitude as the Fluid B thickness and the region of excess charge is distributed over the entire fluid. This situation is not fully compatible with this solution for which the Debye-Hückel approximation was invoked, which requires $\overline{\kappa}_{min} \gtrsim 10$. In this work and as a typical example, we set $\bar{\kappa} = 20$ in all figures.

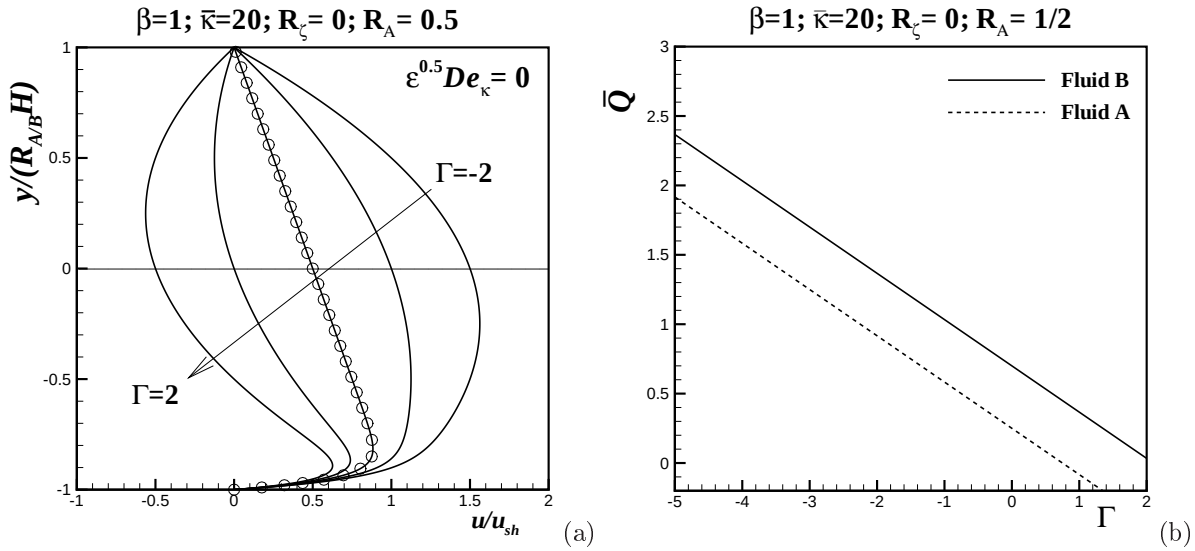

Figure 2: Effect of the driving forces ($\Gamma = -2$, -1, 0, 1 and 2) on dimensionless (a) velocity profiles and (b) volumetric flow rate for Newtonian-Newtonian flow configuration. Symbols represent the data from Afonso et al [14] for ($\beta = 1$, $R_\zeta = 0$ and $\Gamma = 0$).

For $\Gamma = 0$, i.e., when the flow is driven only by electro-osmosis, the velocity profile is a function of the wall distance, of the relative microchannel ratio, $\bar{\kappa}$, of the ratio of zeta potentials, R_ζ, and of the dynamic viscosity ratio as shown earlier by Gao et al [2]. Also,

for a single fluid situation ($\beta = 1$) and in the absence of interface zeta potential ($R_\zeta = 0$) the solution simplifies to the particular case obtained by Afonso et al [14] (no zeta potential in the upper wall and no pressure gradient, cf. Figure 2a). The corresponding effect of the ratio of pressure gradient to electro-osmotic driving forces on the dimensionless flow rate is obvious (cf. Figures 2(b)), increasing with favorable pressure gradients ($\Gamma < 0$), whereas decreasing for flows with adverse pressure gradients ($\Gamma > 0$). Obviously, the flow rate for fluid B is higher because for identical fluids heights fluid B is being forced also by electro-osmosis.

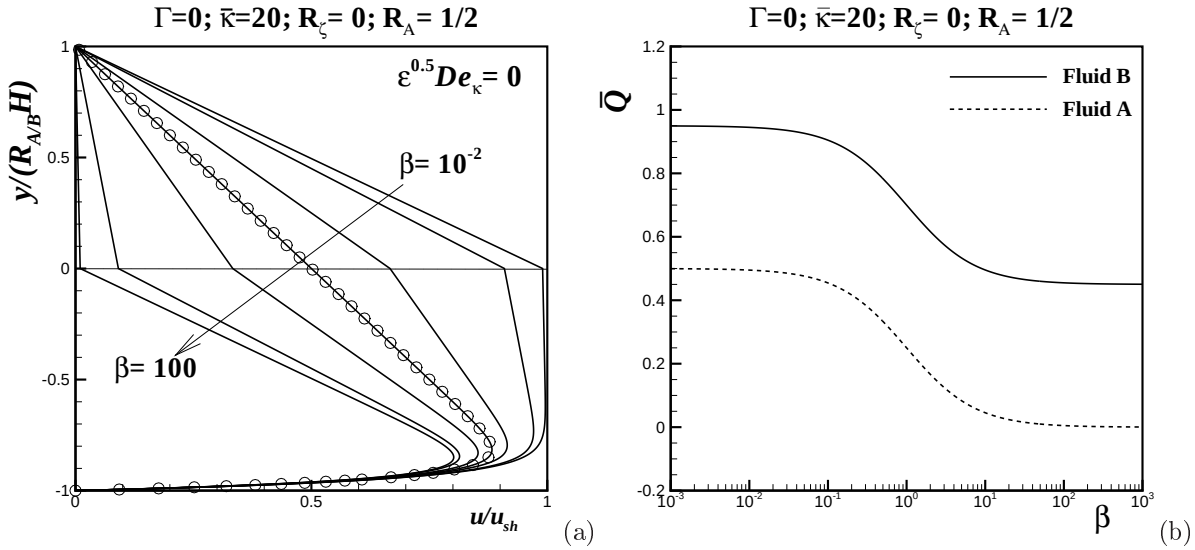

Figure 3: Effect of the dynamic viscosity ratio ($\beta = 10^{-2}$, 10^{-1}, 1, 10 and 100) on dimensionless (a) velocity profiles and (b) volumetric flow rate for Newtonian-Newtonian flow configuration.

Figure 3 shows the different influences of the dynamic viscosity ratio ($\beta \equiv \eta_A/\eta_B$) on the dimensionless velocity profile (a) and on the volumetric flow rate (b). When the dynamic viscosity ratio decreases the dimensionless velocity increases (cf. Figure 3(a)). So, if the viscosity of the conducting fluid is much higher than the viscosity of the nonconducting fluid, an increase in the dimensionless volumetric flow rate is expected, as can be observed in Figure 3(b).

A major effect on the valocity profile is that due to non-zero interfacial zeta potential, as presented in the profiles of Figures 4. When $\zeta_i > 0$, a favorable *extra* drag forcing term arises in the velocity profile at the interface of the two-fluids, leading to a significant increase in the volumetric flow rate, even for $\zeta_i < \zeta_1$. When $\zeta_i < 0$, the adverse localized electrostatic force decreases the pumping action and the corresponding dimensionless flow rate (cf. Figure 4(b)).

Another important effect is due to the holdup of the nonconducting fluid. When the height of the nonconducting fluid is larger than the height of the conducting fluid ($R_A > R_B$), the normalized velocities of both fluids increase, as observed in Figure 5(a). This suggests

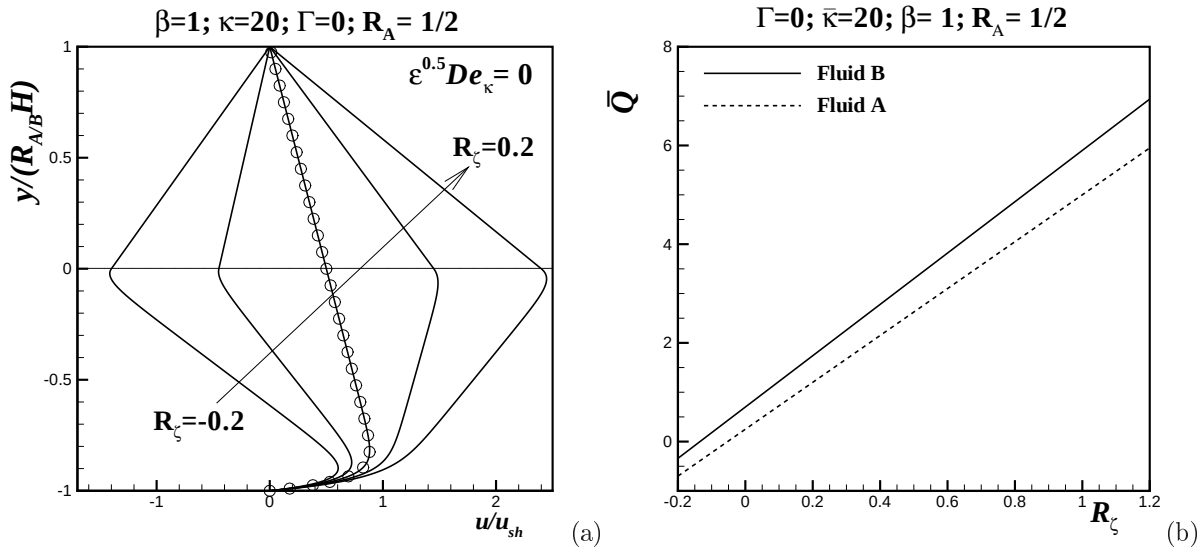

Figure 4: Effect of the ratio of zeta potentials ($R_\zeta = -0.2$, -0.1, 0, 0.1 and 0.2) on dimensionless (a) velocity profiles and (b) volumetric flow rate for Newtonian-Newtonian flow configuration.

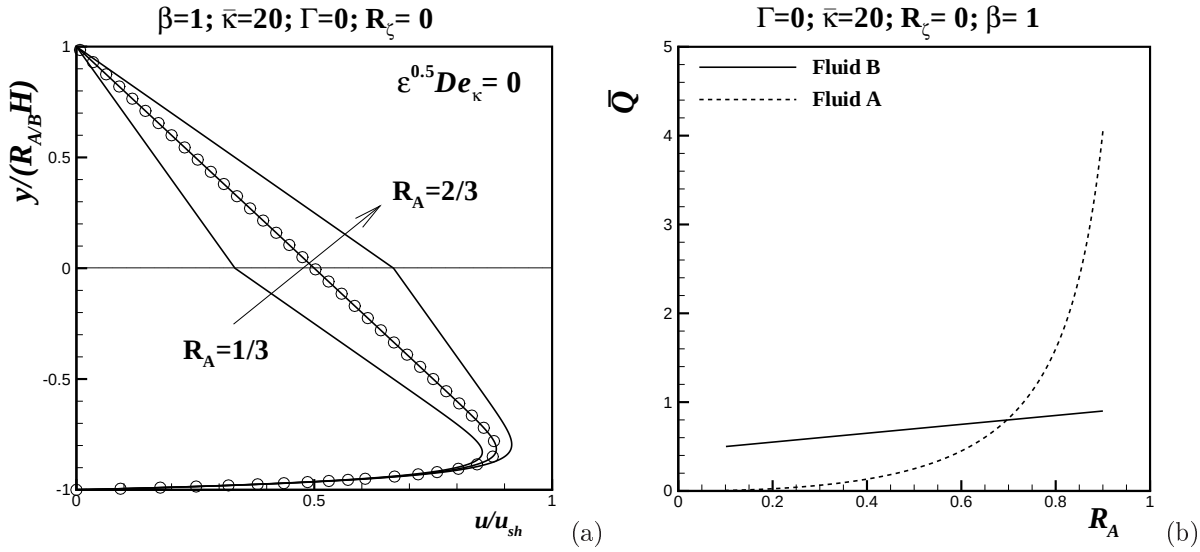

Figure 5: Effect of the nonconducting fluid holdup ($R_A = 1/3$, $1/2$ and $2/3$) on dimensionless (a) velocity profiles and (b) volumetric flow rate for Newtonian-Newtonian flow configuration.

that to obtain higher volumetric flow rates in fluid B, the holdup of the conducting fluid B should be kept small (cf. Figure 5(b)). In fact, as the Helmholtz-Smoluchowski electro-osmotic velocity is independent of the thickness of fluid B, as $R_A \to 1$ the fluid interface palne will tend to coincide with the regions of higher velocity. This conclusion also suggests that a better configuration for an EOF pump would be with the conducting fluid in contact with both the upper and lower walls, with the non conducting fluid in the middleand being dragged like a solid body, i.e., a solid lubrificated by a thin layer of conducting fluid in motion.

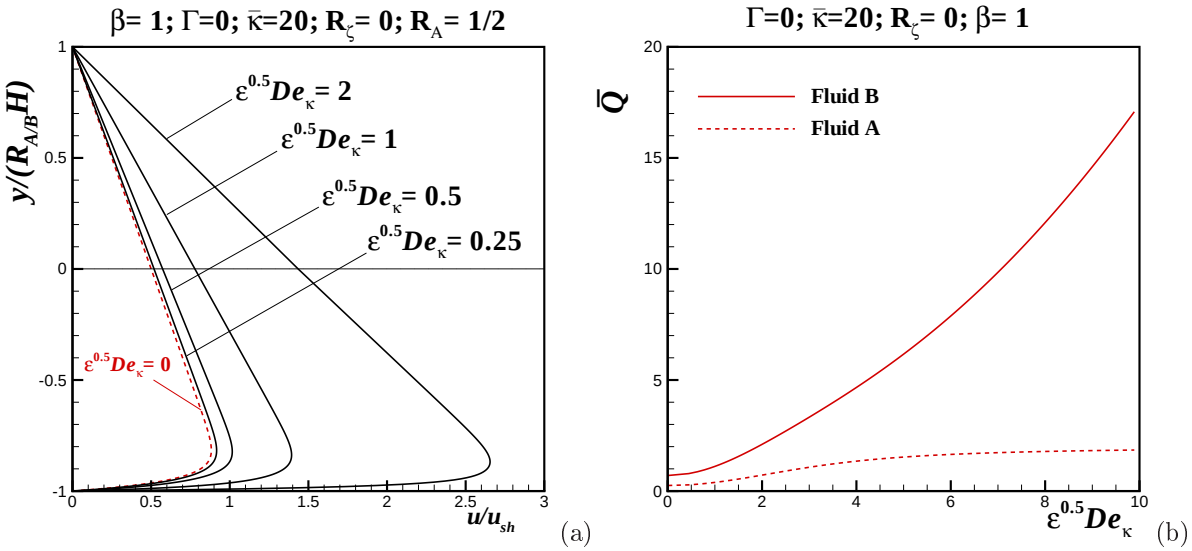

Figure 6: Dimensionless profiles of (a) velocity and (b) volumetric flow rate as function of $\sqrt{\varepsilon}De_\kappa$.

4.2 Newtonian-Viscoelastic EOF pump configuration

For the Newtonian-Viscoelastic flow configuration, the conducting fluid is viscoelastic dragging the nonconducting Newtonian fluid. The Deborah number of the conducting fluid is non-zero ($De_\kappa \neq 0$ and $De_{\kappa A} = 0$), and the velocity profile and the nondimensional boundary condition coefficients are given by

$$\begin{cases} \frac{u^A}{u_{sh}} = \overline{C}_A\left(\overline{y}-1\right) + \frac{1}{2\beta}\Gamma_A\left(\overline{y}^2-1\right) & \text{for} \quad 0 \le \overline{y} \le 1 \\ \text{Eq. (23)} & \text{for} \quad -1 \le \overline{y} \le 0 \\ \overline{C}_A = \frac{R_A}{R_B}\frac{1}{\beta}\left(\sqrt[3]{-\frac{b_1}{2}+\sqrt{\frac{b_1^2}{4}+\frac{a^3}{27}}}+\sqrt[3]{-\frac{b_1}{2}-\sqrt{\frac{b_1^2}{4}+\frac{a^3}{27}}}-\frac{a_1}{3}\right) - \frac{\overline{\kappa}_A}{\beta}\Omega_1^+(0) \\ \overline{C}_B = \sqrt[3]{-\frac{b_1}{2}+\sqrt{\frac{b_1^2}{4}+\frac{a^3}{27}}}+\sqrt[3]{-\frac{b_1}{2}-\sqrt{\frac{b_1^2}{4}+\frac{a^3}{27}}}-\frac{a_1}{3} \end{cases} \tag{35}$$

where $a = a_2 - a_1^2/3$, $b_1 = a_3 - a_1 a_2/3 + 2a_1^3/27$ and the coefficients a_1, a_2 and a_3 are given by

$$
\begin{aligned}
a_1 &= -\frac{3}{2}\Gamma - 2\Omega^-_{1,1}(0) \\
a_2 &= \frac{1}{2}\frac{\overline{\kappa}^2}{\varepsilon De_\kappa^2}\left(\frac{\beta+1}{\beta}\right) + \Gamma^2 + \left(6AB\overline{\kappa} + \frac{3}{2}\Omega^-_{2,1}(0)\right) - 6\frac{\Gamma}{\overline{\kappa}}\left(\Omega^-_{1,2}(0) - \Omega^-_{1,1}(0)\right) \\
a_3 &= -\frac{1}{4}\Gamma\left(1+\Gamma^2\right) - \frac{1}{2}\frac{\overline{\kappa}^2}{\varepsilon De_\kappa^2}\left(\Omega^-_{1,1}(0) - \frac{\overline{\kappa_A}}{\beta}\Omega^+_1(0)\right) - \overline{\kappa}^2\left(\frac{1}{3}\Omega^-_{3,1}(0) + 3AB\Omega^-_{1,1}(0)\right) \\
&\quad + 3\Gamma\left(-AB\overline{\kappa}^2 + \frac{1}{2}\Omega^-_{2,2}(0) - \frac{1}{4}\Omega^+_{2,1}(0) - \frac{\Gamma}{\overline{\kappa}^2}\left(\Omega^-_{1,3}(0) + 2\Omega^-_{1,1}(0) - 2\Omega^+_{1,2}(0)\right)\right)
\end{aligned}
\tag{36}
$$

Figures 6 (a) and (b) present the dimensionless velocity and volumetric flow rate profiles as a function of $\sqrt{\varepsilon}De_\kappa$, respectively. We can see that increasing the elasticity of the conducting fluid, more than doubles the velocities due to shear-thinning effects within the EDL layer thus raising the velocity value of the bulk transport in the core of the channel. This also helps to increase the shear rates near the bottom wall and at the two fluids interface, increasing the dragging of the nonconducting fluid by the hydrodynamic viscous forces at the interface. Consequently there is a significant increase in the dimensionless volumetric flow rate (cf. Figure 6(b)).

As we can also see in Figure 6 (a), in the absence of pressure gradient the EDL acts like a plate in pure Couette flow, transmitting a constant shear stress across the channel.

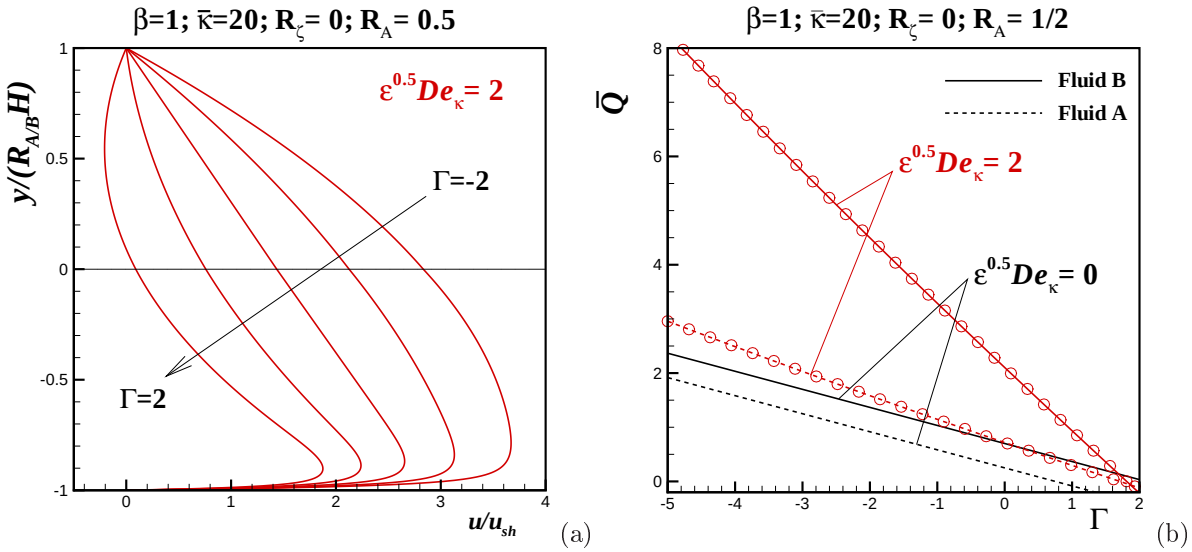

Figure 7: Effect of the driving forces ($\Gamma = -2$, -1, 0, 1 and 2) on dimensionless (a) velocity profiles and (b) volumetric flow rate for Newtonian-Viscoelastic flow configuration.

Figure 7 shows the dimensionless velocity profiles (a) and volumetric flow rate (b) at $\sqrt{\varepsilon}De_\kappa = 2$ (for comparison the Newtonian results of Figures 2 are also presented) to

illustrate the effect of Γ. A favorable pressure gradient ($\Gamma < 0$) helps increase the flow rate and makes velocity profiles fuller. By using pressure, the dragging effect at the interface is helped by the pressure forcing which affects directly the two fluids. The beneficial shear-thinning effect is clear in the large increase in the flow rate of Figure 7(b).

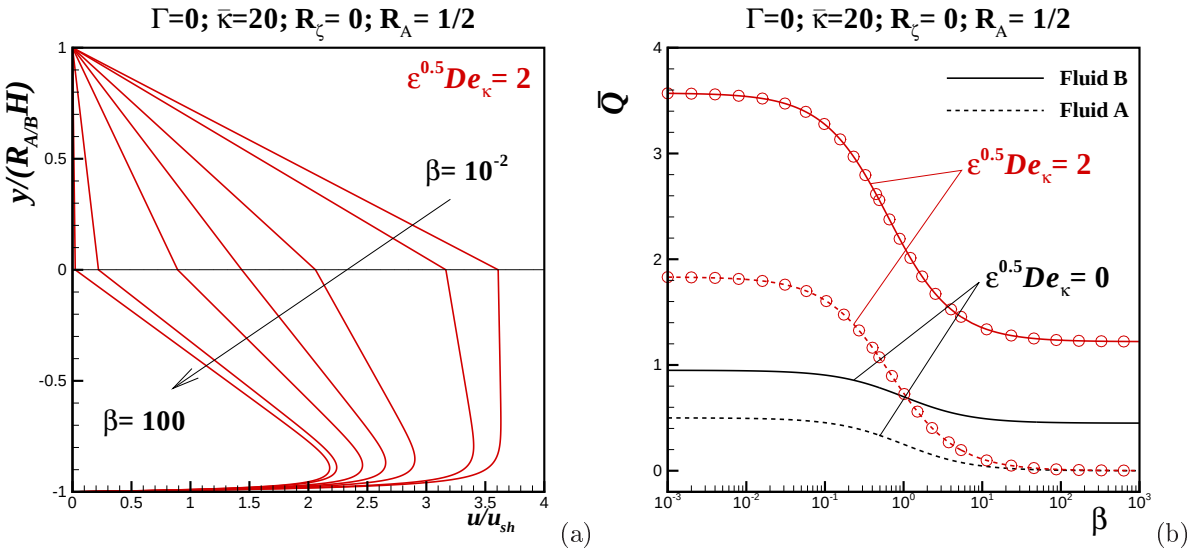

Figure 8: Effect of the dynamic viscosity ratio ($\beta = 10^{-2}$, 10^{-1}, 1, 10 and 100) on dimensionless (a) velocity profiles and (b) volumetric flow rate for Newtonian-Viscoelastic flow configuration.

As for the Newtonian-Newtonian flow configuration, decreasing β leads to an increase in velocity profiles and the volumetric flow rate, which is further increased by shear-thinning effects (cf. Figure 8(a) and (b) and compare with Figure 3). When using a viscoelastic fluid as conducting fluid it is natural to have a more viscous fluid than the Newtonian nonconducting fluid, which leads to an *optimal* flow situation.
The effects of the fluid A holdup (R_A) and of the ratio of zeta potentials (R_ζ) are similar to what was seen before, but now the viscoelastic flow exhibits a shear-thinning viscosity and the velocities have increased significantly near the bottom wall (see the higher values of u/u_{sh}) leading to higher volumetric flow rates of Figures 9 and 10, than in the corresponding constant viscosity case.

5 Conclusions

An analytical solution of the steady two-fluid electro-osmotic stratified flow in a planar microchannel is presented by assuming a planar interface between the two viscoelastic immiscible fluids. The PTT fluid model [11, 12] was used, and the effects of fluid rheology, viscosity ratio, fluid holdup and interfacial zeta potential were analyzed to show the viability of this technique.

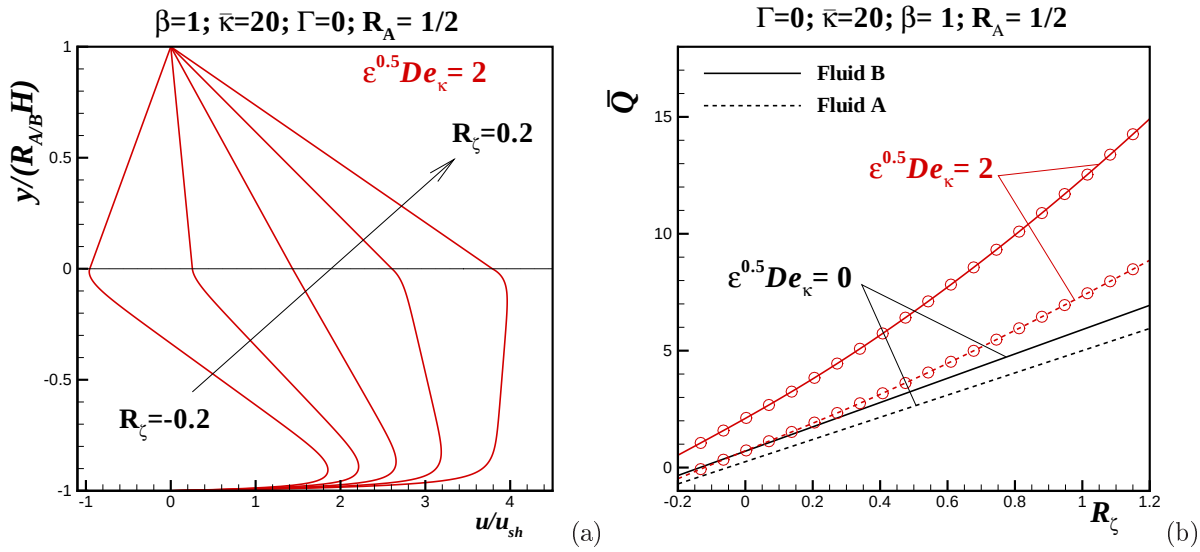

Figure 9: Effect of the ratio of zeta potentials (R_ζ = −0.2, -0.1, 0, 0.1 and 0.2) on dimensionless (a) velocity profiles and (b) volumetric flow rate for Newtonian-Viscoelastic flow configuration.

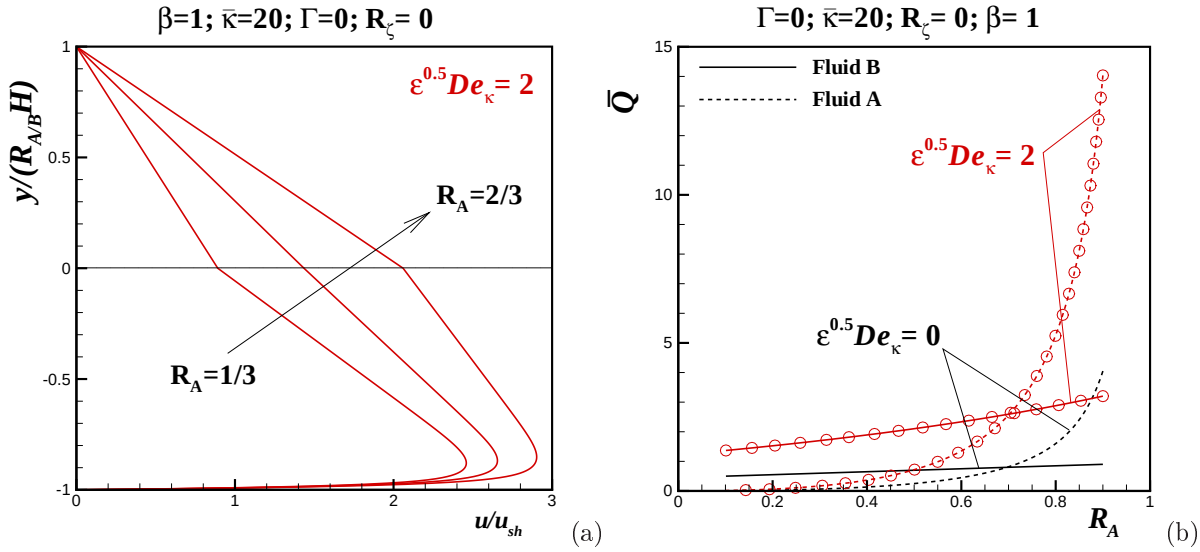

Figure 10: Effect of the nonconducting fluid holdup (R_A = 1/3, 1/2 and 2/3) on dimensionless (a) velocity profiles and (b) volumetric flow rate for Newtonian-Viscoelastic flow configuration.

The flow can be induced by a combination of both electrical and pressure potentials, but in addition to the single contributions from these two mechanisms, when the conducting fluid is viscoelastic, there is an extra term in the velocity profile that simultaneously combines both effects, which is absent from conducting Newtonian fluids where the linear superposition principle applies. Hence, for non-linear viscoelastic fluids the superposition principle is not valid.
This work demostrated that higher volumetric flow rates of a nonconducting Newtonian fluid can be acheived in EOF pumping when the conducting fluid is viscoelastic rather than Newtonian, due to the increasing of the shear-thinning effects.

6 Acknowledgments

The authors would like to acknowledge financial support of FCT through projects PTDC/ EQU-FTT/71800/2006, PTDC /EQU-FTT/70727/2006 and scholarship SFRH/BD/28828 /2006 (A. M. Afonso).

REFERENCES

[1] A. Brask, G. Goranovic, H. Bruus, "A novel electro-osmotic pump design for non-conducting liquids: theoretical analysis of flow rate–pressure characteristics and stability", *Tech. Proc. Nanotech.*, Vol. **1**, pp. 190–193, (2003).

[2] Y. Gao, T. N. Wong, C. Yang, K. T. Ooi, "Two-fluid electroosmotic flow in microchannels", *J. Colloid Interface Sci.*, Vol **285**, pp. 306–314, (2005).

[3] C.-H. Chen , J.G. Santiago, "A planar electroosmotic micropump". *J. Microelectromech Syst.*, Vol. **11**, pp 672-683, (2002).

[4] X. Xuan, D. Li, "Analysis of electrokinetic flow in microfluidic networks". *J. Micromech. Microeng.*, Vol. **14**, pp. 290-298, (2004).

[5] X. Wang, C. Cheng, S. Wang, S. Liu, "Electroosmotic pumps and their application in microfluidic systems". *Microfluid. Nanofluid.*, Vol. **6**, pp. 145-162, (2009).

[6] S. Das and S. Chakraborty, "Analytical solutions for velocity, temperature and concentration distribution in electroosmotic microchannel flows of a non-Newtonian biofluid", *Analytica Chimica Acta*, Vol. **559**, pp. 15–24, (2006).

[7] S. Chakraborty, "Electroosmotically driven capillary transport of typical non-Newtonian biofluids in rectangular microchannels", *Anal. Chimica Acta*, Vol. **605**, pp. 175–184, (2007).

[8] C. L. A. Berli and M. L. Olivares, "Electrokinetic flow of non-newtonian fluids in microchannels". *J. Colloid Interface Sci.*, Vol. **320**, pp. 582-589, (2008).

[9] A. M. Afonso, M. A. Alves and F. T. Pinho, "Analytical solution of mixed electro-osmotic/pressure driven flows of viscoelastic fluids in microchannels", *J. Non-Newtonian Fluid. Mech.*, doi:10.1016/j.jnnfm.2009.01.006, (2009).

[10] R. F. Probstein, *Physicochemical Hydrodynamics: An introduction*. Second edition, Wiley Interscience, Hoboken (2003).

[11] N. Phan-Thien, R. I. Tanner, "New constitutive equation derived from network theory". *J. Non-Newtonian Fluid Mech.*, Vol. **2**, pp. 353-365, (1977).

[12] N. Phan-Thien, "A non-linear network viscoelastic model". *J. Rheo.*, Vol. **22**, pp. 259, (1978).

[13] R. B. Bird, P. J. Dotson, N. L. Johnson, "Polymer solution rheology based on a finitely extensible bead-spring chain model". *J. Non-Newtonian Fluid Mech.*, Vol. **7**, pp. 213-235, (1980).

[14] A. M. Afonso, M. A. Alves and F. T. Pinho, "Electro-osmotic flows of viscoelastic fluids in microchannels under asymmetric zeta potential", in preparation, (2009).

[15] C. Yang and D. Li, "Electrokinetic effect on pressure-driven liquid flows in rectangular microchannels". *J. Colloid Interface Sci.*, Vol. **194**, pp. 95-107, (1997).

[16] F. T. Pinho and P. J. Oliveira, "Axial annular flow of a nonlinear viscoelastic fluid—an analytical solution". *J. Non-Newtonian Fluid Mech.*, Vol. **93**, pp. 325–337, (2000).

[17] M. A. Alves, F. T. Pinho and P. J. Oliveira, "Study of steady pipe and channel flows of a single-mode Phan Thien–Tanner fluid". *J. Non-Newtonian Fluid Mech.*, Vol. **101**, pp. 55–76, (2001).